THE JOURNAL OF PHYSICAL CHEMISTRY Letters

Letter

pubs.acs.org/JPCL

Inorganic Halide Perovskites for Efficient Light-Emitting Diodes

Natalia Yantara,[†] Saikat Bhaumik,[†] Fei Yan,[‡] Dharani Sabba,[†] Herlina A. Dewi,[†] Nripan Mathews,*[,†,§] Pablo P. Boix,*[,†] Hilmi Volkan Demir,[‡] and Subodh Mhaisalkar[†,§]

[†]Energy Research Institute@NTU (ERI@N), Research TechnoPlaza, X-Frontier Block, Level 5, 50 Nanyang Drive, 637553 Singapore

[‡]LUMINOUS! Center of Excellence for Semiconductor Lighting and Displays, School of Electrical and Electronic Engineering, School of Physical and Mathematical Sciences, Nanyang Technological University, 50 Nanyang Avenue, 639798 Singapore

[§]School of Materials Science and Engineering, Nanyang Technological University, 50 Nanyang Avenue, 639798 Singapore

Supporting Information

ABSTRACT: Lead-halide perovskites have transcended photovoltaics. Perovskite light-emitting diodes (PeLEDs) emerge as a new field to leverage on these fascinating semiconductors. Here, we report the first use of completely inorganic $CsPbBr_3$ thin films for enhanced light emission through controlled modulation of the trap density by varying the CsBr-$PbBr_2$ precursor concentration. Although pure $CsPbBr_3$ films can be deposited from equimolar CsBr-$PbBr_2$ and CsBr-rich solutions, strikingly narrow emission line (17 nm), accompanied by elongated radiative lifetimes (3.9 ns) and increased photoluminescence quantum yield (16%), was achieved with the latter. This is translated into the enhanced performance of the resulting PeLED devices, with lower turn-on voltage (3 V), narrow electroluminescence spectra (18 nm) and higher electroluminescence intensity (407 Cd/m^2) achieved from the CsBr-rich solutions.

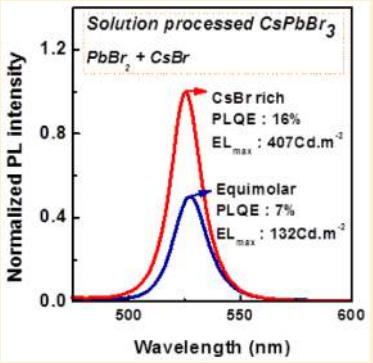

The use of organic−inorganic lead halide ($MPbX_3$ with X: Cl, Br, I and M: $HC(NH_2)_2$, CH_3NH_3) perovskite materials has enabled a major breakthrough in solution-processed photovoltaic devices, attaining record high power conversion efficiencies above 20%.[1] This remarkable achievement is attributed to their excellent optoelectrical properties such as long diffusion lengths[2−5] and low defect densities,[6] resulting in low recombination rates.[7] With these outstanding characteristics, perovskites have the potential to be an important material for the field of light emission.[8] Recently, a strong photoluminescence quantum yield (PLQY) up to 70%[9] has been measured for $CH_3NH_3PbI_3$, and it has been successfully incorporated into PeLEDs.[10] Following a similar approach, visible-light-emitting devices from solution-processed $CH_3NH_3PbBr_3$ were first reported with threshold voltage, highest luminescence, and external quantum efficiency of 3.3 V, 364 $Cd{\cdot}m^{-2}$, and 0.1%, respectively.[11] The peak electroluminescence wavelength can be tuned by changing the halide material; for example, the replacement of I by Br allowed the peak emission wavelength to shift from 517 to 754 nm.[11] The use of a blend of perovskite and nonconducting polymers helps to produce pinhole-free films, reducing the nonradiative losses and improving the quantum efficiency to 1.2%.[12] Despite its successful integration for PeLEDs application,[11−13] the use of organic−inorganic lead halide materials can be hampered by its thermal stability.[14−16]

Alternative materials that employ inorganic cations, such as Cs^+, could be pursued to enhance thermal stability of the devices. Thermally stable $CsPbBr_3$ (up to 250 °C in air) can be deposited via solution process[14,17] followed by solid-state reaction crystallizing in an orthorhombic (*Pnma*) space group with a distorted perovskite structure.[18] The optoelectronic properties of $CsPbBr_3$ have been studied in depth, including balanced electron and hole mobility-lifetime product ($\mu\tau$), long electron mobility (1000 $cm^2/V{\cdot}s$) and lifetime (2.5 μs),[18] small exciton binding energy (35 meV), and stimulated emission at room temperature.[19] These attractive features of $CsPbBr_3$, along with its thermal stability, have opened the possibility of using these materials for PeLED applications, with some reports in the quantum dot form;[20] however, typically fast free exciton emission decay (∼1 ns), which stems from strong nonradiative energy transfer to the trap states,[21,22] represents a fundamental challenge for this material system in making PeLEDs. Hence, controlling and reducing the trap density in the film is the key to enhancing $CsPbBr_3$-based PeLEDs.

In this paper, to address this problem, we studied low-temperature (70 °C) solution-processed $CsPbBr_3$ for enhanced light emission by decreasing their trap density by controlling their precursor concentration and demonstrated the feasibility of using their thin-films as an emissive layer in PeLEDs. By using CsBr-rich solution, the trap density of the resulting $CsPbBr_3$ film was reduced, which has therefore increased luminescence (L) and decreased the turnon voltage of the PeLED. Consequently, a maximum level of 407 Cd/m^2 (at 7.2

Received: September 11, 2015
Accepted: October 16, 2015
Published: October 16, 2015

DOI: 10.1021/acs.jpclett.5b02011
J. Phys. Chem. Lett. 2015, 6, 4360−4364

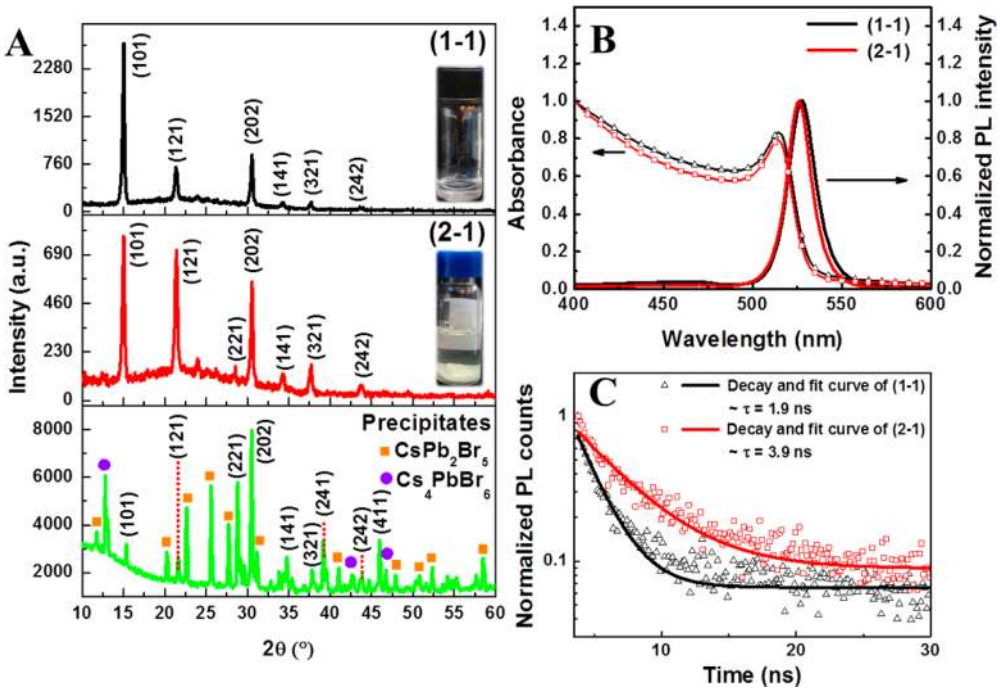

Figure 1. XRD spectra (A), absorption and photoluminescence spectra (B), and time-resolved photoluminescence decay curves (C) of $CsPbBr_3$ films (1−1) and (2−1) grown from different solution ratios. The images of the equimolar and CsBr-rich solutions ($CsBr/PbBr_2$ ratio of 2.0) were presented in the inset of the XRD spectra.

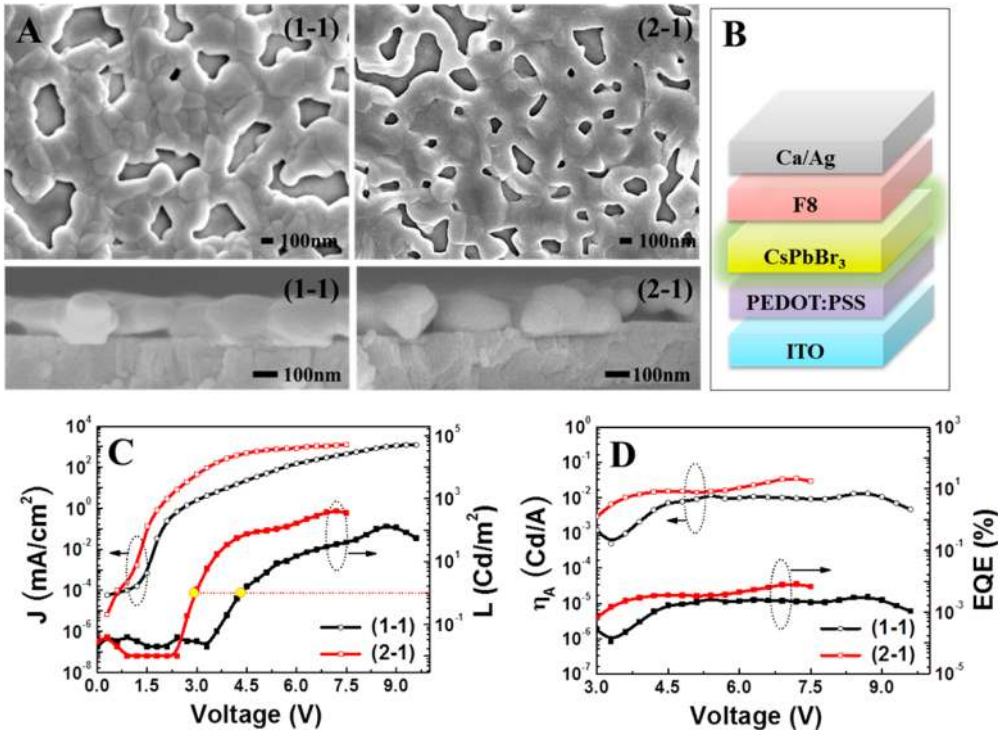

Figure 2. Topographic and cross-sectional images of (1−1) and (2−1) samples (A) together with the generic schematic diagram of the devices (B). *J*−*V*−*L* curves (C) and current efficiency (η_A) and external quantum efficiency (EQE) versus driving voltage curves (D) of all samples.

V) with 3.0 V turnon voltage could be achieved with these solution-processed $CsPbBr_3$-based PeLEDs.

The $CsPbBr_3$ thin films were spin-casted from solutions with varied $CsBr/PbBr_2$ concentrations (i.e., 0.8, 1.0, 2.0, and 3.0) in DMSO solvent. The films were then annealed at 70 °C to evaporate the solvent. The full studies on the effect of varied $CsBr/PbBr_2$ ratios on the crystal structure and optoelectronic properties of the resulting films can be found in the Supporting Information. Clear solution was observed when using equimolar CsBr-$PbBr_2$ solution (named 1−1). The X-ray diffraction (XRD) patterned of the set of films spin-coated from the equimolar solution revealed that these consist of polycrystalline $CsPbBr_3$ phase (Figure 1a). These match well with orthorhombic (*Pnma*) crystal structure of $CsPbBr_3$ as

DOI: 10.1021/acs.jpclett.5b02011
J. Phys. Chem. Lett. 2015, 6, 4360−4364

previously[18] reported, with the lattice parameters of a = 8.26(3) Å, b = 11.79(5) Å, and c = 8.19(3) Å. The (1−1) films were preferentially oriented toward (101) direction. In the case of 2.0 CsBr/$PbBr_2$ ratio solution, white precipitates were formed even after stirring for >12 h. The precipitates were dried at 70 °C and the XRD spectra of the precipitates indicated the existence of $CsPb_2Br_5$, Cs_4PbBr_6, and $CsPbBr_3$ crystallites (Figure 1a). The films spun from the supernatant of the 2.0 CsBr/$PbBr_2$ solution (named 2−1) were transparent and gradually transformed to yellow film after 5 min drying in N_2 ambient at room temperature. This indicates the relatively slow crystallization of (2−1) films as compared with (1−1) films, which transform to yellow immediately after spin-coating. The XRD analysis revealed that (2−1) films consist of orthorhombic $CsPbBr_3$ crystal. The lattice parameters are a = 8.25(5) Å, b = 11.79(1) Å, and c = 8.20(1) Å, with no preferential growth that were noticed on these (2−1) films.

Both (1−1) and (2−1) films present an absorption band edge of 530 nm, while their PL emission peaks are located at ca. 527 nm, each with a full width at half-maximum (fwhm) of 17 nm (Figure 1b). The insignificant difference between the absorbance edges and that between the PL peaks suggests that the PL emission of $CsPbBr_3$ originates from direct recombination across the band edge; however, (2−1) films exhibit significantly higher PLQY compared with (1−1) films (16 and 7%, respectively). Their PL decay lifetimes were extracted from their respective time-resolved PL spectrum (Figure 1c), using numerical exponential fitting as follows[23]

$$y(t) = A \cdot e^{\left(\frac{-(t-t_o)}{\tau}\right)}$$

where $y(t)$ is the time-dependent PL intensity, y_o is the initial PL intensity, A is the distribution coefficient, $(t - t_o)$ is the time axis starting from t_o, and τ stands for the characteristic PL decay lifetime.

The characteristic PL lifetime (τ) for (1−1) films is 1.9 ns, and it is 3.9 ns for (2−1) films. Together with the higher PLQY observed in (2−1) films, their measured longer PL lifetime indicates low nonradiative defect densities as compared with (1−1) samples. The exemplary morphological and cross-sectional images of the (1−1) and (2−1) samples are shown in Figure 2A. Approximately 200 nm thick with 85−90% film coverage (obtained from ImageJ analysis) was obtained for all samples. Increasing the CsBr content of the solution does not change the morphology, coverage, and grain size of the spin-coated films. Therefore, this improvement is tentatively attributed to the reduction of halogen vacancies (V_{Br}). This is supported by previous theoretical reports, where density functional theory (DFT) indicates that the presence of V_{Br} on $CsPbBr_3$ generates defects within the band gap, which could act as recombination centers.[24] The deposition via CsBr-rich solution may decrease the probability of V_{Br} formation on the films and hence reduce the nonradiative defect densities.

The schematic diagram of the fabricated PeLED devices consists of an ITO-coated glass with PEDOT:PSS serving as the hole-injecting material, $CsPbBr_3$ perovskite as the emitter film, poly(9,9-di-*n*-octylfluorenyl-2,7-diyl) (F8) as the electron injecting material, and an evaporated contact of Ca and Al, as illustrated in Figure 2B. Figure 2C presents the current density and luminescence versus driving voltage (J−V−L curves) for all samples under forward bias. Table 1 summarized the PeLED performances for all samples. The devices display a turnon voltage (V_{th}) of 1.6 and 1.3 V for (1−1) and (2−1), respectively. Lower differential resistance (dV/dJ) was observed for devices made of (2−1) film, suggesting better charge transport. Devices with (2−1) showed lowest turn-on voltage of luminescence (3.0 V) with maximum L (407 Cd/m^2). Approximately 2 V discrepancy between the current turn-on voltage and the turn-on voltage for the electroluminescence were observed for all devices. This indicates that there is a mismatch in the injection barrier of holes and electrons in the devices.[25]

Table 1. List of the Set of Devices and Their Light-Emitting Diode Performances

$CsBr-PbBr_2$ molar ratio	V_{th} (V)	L_{max} (Cd/m^2)	$\eta_{A_{max}}$ (Cd/A)
1:1	4.3	132	0.013
2:1	3.0	407	0.035

To further understand the fundamental differences between both fabrication processes, we analyzed the energetics of the resulting perovskite films; however, photoelectron spectroscopy in air (PESA) plot (Figure S1) films resulted in a comparable ionization potential for both methods, thereby signifying similar driving force for carrier injection. This suggests that the lower defect density of (2−1) films has a double effect: On the one hand, it reduces the nonradiative recombination in the emissive layer, thus increasing the radiative one. On the other hand, it enhances the carrier injection efficiency and consequently reduces the turn-on voltages for the devices with (2−1) film. High carrier injection can promote balanced recombination with and, as a result, increase the luminance intensity as well.[26] This is confirmed in Figure 2D, which reveals that the devices with (2−1) exhibit better current efficiency (η_A) and external quantum efficiency (EQE) with the maximum point of 0.035 Cd/A and 0.008%, respectively, when operated at 7.2 V. The low η_A observed is probably due to high driving J, which might be due to the leakage current, possibly resulting from pin holes on the emitter films (Figure 2A). Solar cells based on (1−1) and (2−1) films were fabricated to verify the improvement of the perovskite optoelectrical properties. (See the Supporting Information.) As in the PeLED case, the reduction of the nonradiative recombination and enhancement of the charge transport resulted in higher performance for the (2−1) devices due to better V_{oc}, J_{sc}, and FF.

Figure 3A presents the electroluminescence spectra of the PeLEDs devices peaking at 527 nm with a fwhm of 18 nm, which is in agreement with the PL spectra of these $CsPbBr_3$ films, while no emission spectra from F8 is detected. The electroluminescence spectrum is independent of the external bias (Figure 3B).

Remarkably, the exposure of the (2−1) films to the ambient conditions (relative humidity ∼70%) does not degrade its PLQY; on the contrary, it shows a slightly increase (Figure 4) probably due to the surface passivation by O_2 and H_2O molecules.[27] These preliminary results show a promising stability of the material, in contrast with previous reports on hybrid organic−inorganic perovskites. PLQY enhancement with prolong air exposure was observed for all films deposited from equimolar and CsBr-rich samples; however, extended air exposure decreases the PLQY of the films with $PbBr_2$-rich samples, which might be attributed to the presence of $CsPb_2Br_5$ impurity that could affect the stability of $CsPbBr_3$ (Figure S4).

In summary, here the first account of solution-processed $CsPbBr_3$-based light-emitting diode is presented. The demon-

DOI: 10.1021/acs.jpclett.5b02011
J. Phys. Chem. Lett. 2015, 6, 4360−4364

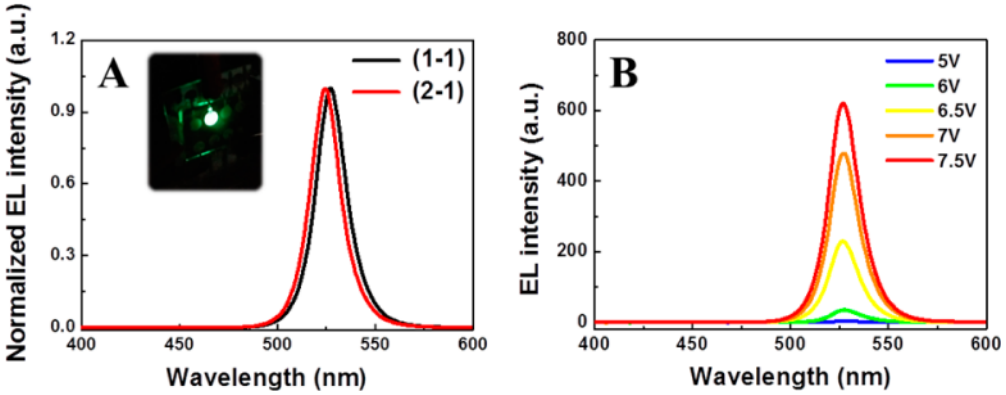

Figure 3. EL spectra of all samples (A) together with the EL spectra of devices with (2−1) films at different driving voltages: 5, 6, 6.5, 7, and 7.5 V (B).

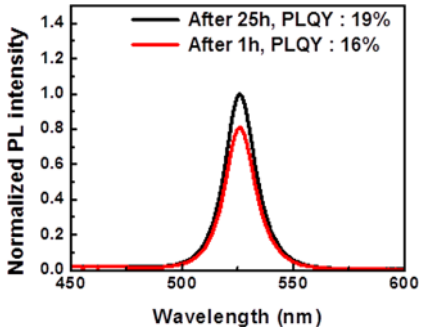

Figure 4. PLQY evolution of (2−1) films measured at different times after storing in air with relative humidity of ∼70%.

strated $CsPbBr_3$ PeLED possesses stable and narrow electroluminescence spectra (18 nm). The use of CsBr-rich solution for the $CsPbBr_3$ formation results in a reduced trap density, as indicated by the longer PL lifetime and higher PLQY. The reduction of the defects density leads to a lower turnon voltage (3 V) and a higher luminescence (L_{max} = 407 Cd/m^2) attributed to a balanced charge recombination because traps can hinder the carrier injection to the $CsPbBr_3$. Future work will focus on further improving the device performance and stability. These findings indicate that low-temperature solution-processed $CsPbBr_3$ holds great promise for high-performance PeLEDs.

EXPERIMENTAL METHODS

Device Fabrication. The PeLED devices are fabricated on top of indium-doped tin oxide (ITO, 7 $\Omega \cdot cm^{-2}$) coated glass substrates. The samples were cleaned by sonication in decon soap, distilled water, and ethanol solution. The samples were then dried and cleaned with oxygen plasma for 15 min. A layer of PEDOT:PSS (Clevios P VP Al 4083) was spin-coated at 3000 rpm for 60 s and annealed at 130 °C for 15 min in air to remove water from the PSS shell of the PEDOT:PSS grains. Equimolar CsBr (Aldrich, 99.9%) and $PbBr_2$ (Aldrich, ≥ 98%) solution and CsBr-rich solution (CsBr:$PbBr_2$ molar ratio of 2:1) were prepared using DMSO solvent. The solutions were stirred for 5 h at room temperature. Precipitates were formed in the CsBr-rich solutions. Subsequently, spin-coating of the filtered solutions at 2000 rpm for 60 s was carried out to form a thin-film on top of PEDOT:PSS coated substrate. Films deposited from equimolar CsBr-$PbBr_2$ solution were called (1−1), while the films formed from CsBr-rich solution were named (2−1). The samples were dried at room temperature for 30 min, followed by annealing at 70 °C for 30 min. Poly(9,9-di-*n*-octylfluorenyl-2,7-diyl) (Aldrich, F8) was dissolved in chlorobenzene (10 mg/mL) and spun at 4000 rpm for 30 s. Finally, Ca (20 nm) and Ag (80 nm) were thermally evaporated at a base pressure of 1 × 10^{-5} Torr to complete the process of device fabrication. The devices were encapsulated inside the glovebox and then tested outside. The final device active area was 7 mm^2.

Device Characterization. The current density−voltage (J−V) characteristics of the PeLED devices were recorded with Agilent B2902A precision source/measure unit, and luminous output of the devices was measured by LS-110 Konica Minolta luminance meter. All of these instruments were connected to a computer and operated through LabVIEW software. The spectral response of EL emission was collected by Shimadzu RF-5301pc spectrofluorophotometer after blocking the excitation beam. The absolute PL quantum yields (PLQYs) were recorded using Ocean-optics USB4000 spectrometer with an integrated sphere excited at a wavelength of 400 nm. The PL lifetime was recorded with DCS 120 Becker & Hickl confocal scanning FLIM system at an excitation wavelength of 375 nm. Cross-sectional and morphological imaging was carried out using field-emission scanning electron microscopy (FESEM, JEOL JSM-7600F). X-ray diffraction analysis was carried out with XRD Bruker D8 Advance.

ASSOCIATED CONTENT

Supporting Information

The Supporting Information is available free of charge on the ACS Publications website at DOI: 10.1021/acs.jpclett.5b02011.

Photoelectron spectroscopy in air (PESA) spectra of $CsPbBr_3$ films from various CsBr/$PbBr_2$ ratios. Study on the stability of $CsPbBr_3$-based PeLED impact of CsBr/$PbBr_2$ ratio on the optoelectronic properties of the film. Reproducibility of PeLED effect of CsBr/$PbBr_2$ ratio on the solar cell performances. (PDF)

AUTHOR INFORMATION

Corresponding Authors

*E-mail: PBPablo@ntu.edu.sg.
*E-mail: Nripan@ntu.edu.sg.

Notes

The authors declare no competing financial interest.

DOI: 10.1021/acs.jpclett.5b02011
J. Phys. Chem. Lett. 2015, 6, 4360−4364

■ ACKNOWLEDGMENTS

We acknowledge the funding from Singapore NRF through the Competitive Research Program: NRF-CRP4-2008-03 and NRF-CRP14-2014-03 as well as from NTU-A*STAR Silicon Technologies Centre of Excellence under the program grant no. 112 3510 0003.

■ REFERENCES

(1) Yang, W. S.; Noh, J. H.; Jeon, N. J.; Kim, Y. C.; Ryu, S.; Seo, J.; Seok, S. Il. High Performance Photovoltaic Perovskite Layers Fabricated through Intramolecular Exchange. *Science* **2015**, *348*, 1234.

(2) Edri, E.; Kirmayer, S.; Mukhopadhyay, S.; Gartsman, K.; Hodes, G.; Cahen, D. Elucidating the Charge Carrier Separation and Working Mechanism of $CH_3NH_3PbI_{(3-x)}Cl_{(x)}$ Perovskite Solar Cells. *Nat. Commun.* **2014**, *5*, 3461.

(3) Xing, G.; Mathews, N.; Sun, S.; Lim, S. S.; Lam, Y. M.; Grätzel, M.; Mhaisalkar, S.; Sum, T. C. Long-Range Balanced Electron- and Hole-Transport Lengths in Organic-Inorganic $CH_3NH_3PbI_3$. *Science* **2013**, *342*, 344−347.

(4) Stranks, S. D.; Eperon, G. E.; Grancini, G.; Menelaou, C.; Alcocer, M. J. P.; Leijtens, T.; Herz, L. M.; Petrozza, A.; Snaith, H. J. Electron-Hole Diffusion Lengths Exceeding 1 Micrometer in an Organometal Trihalide Perovskite Absorber. *Science* **2013**, *342*, 341−344.

(5) Sun, S.; Salim, T.; Mathews, N.; Duchamp, M.; Boothroyd, C.; Xing, G.; Sum, T. C.; Lam, Y. M. The Origin of High Efficiency in Low-Temperature Solution-Processable Bilayer Organometal Halide Hybrid Solar Cells. *Energy Environ. Sci.* **2014**, *7*, 399.

(6) Xing, G.; Mathews, N.; Lim, S. S.; Yantara, N.; Liu, X.; Sabba, D.; Grätzel, M.; Mhaisalkar, S.; Sum, T. C. Low-Temperature Solution-Processed Wavelength-Tunable Perovskites for Lasing. *Nat. Mater.* **2014**, *13*, 476−480.

(7) Wehrenfennig, C.; Eperon, G. E.; Johnston, M. B.; Snaith, H. J.; Herz, L. M. High Charge Carrier Mobilities and Lifetimes in Organolead Trihalide Perovskites. *Adv. Mater.* **2014**, *26*, 1584−1589.

(8) Stranks, S. D.; Snaith, H. J. Metal-halide perovskites for photovoltaic and light-emitting devices. *Nat. Nanotechnol.* **2015**, *10*, 391−402.

(9) Deschler, F.; Price, M.; Pathak, S.; Klintberg, L. E.; Jarausch, D.; Higler, R.; Huttner, S.; Leijtens, T.; Stranks, S. D.; Snaith, H. J.; et al. High Photoluminescence Efficiency and Optically Pumped Lasing in Solution-Processed Mixed Halide Perovskite Semiconductors. *J. Phys. Chem. Lett.* **2014**, *5*, 1421.

(10) Jaramillo-Quintero, O. a.; Sanchez, R. S.; Rincon, M.; Mora-Sero, I. Bright Visible-Infrared Light Emitting Diodes Based on Hybrid Halide Perovskite with Spiro-OMeTAD as a Hole-Injecting Layer. *J. Phys. Chem. Lett.* **2015**, *6*, 1883−1890.

(11) Tan, Z.-K.; Moghaddam, R. S.; Lai, M. L.; Docampo, P.; Higler, R.; Deschler, F.; Price, M.; Sadhanala, A.; Pazos, L. M.; Credgington, D.; et al. Bright Light-Emitting Diodes Based on Organometal Halide Perovskite. *Nat. Nanotechnol.* **2014**, *9*, 687−692.

(12) Li, G.; Tan, Z.-K.; Di, D.; Lai, M. L.; Jiang, L.; Lim, J. H.; Friend, R. H.; Greenham, N. C. Efficient Light-Emitting Diodes Based on Nano-Crystalline Perovskite in a Dielectric Polymer Matrix. *Nano Lett.* **2015**, *15*, 2640−2644.

(13) Kim, Y.-H.; Cho, H.; Heo, J. H.; Kim, T.-S.; Myoung, N.; Lee, C.-L.; Im, S. H.; Lee, T.-W. Multicolored Organic/Inorganic Hybrid Perovskite Light-Emitting Diodes. *Adv. Mater.* **2015**, *27*, 1248−1254.

(14) Kulbak, M.; Cahen, D.; Hodes, G. How Important Is the Organic Part of the Lead Halide Perovskite Photovoltaic Cells? Efficient $CsPbBr_3$ Cells. *J. Phys. Chem. Lett.* **2015**, *6*, 2452−2456.

(15) Dualeh, A.; Gao, P.; Seok, S. Il; Nazeeruddin, M. K.; Grätzel, M. Thermal Behavior of Methylammonium Lead-Trihalide Perovskite Photovoltaic Light Harvesters. *Chem. Mater.* **2014**, *26*, 6160−6164.

(16) Baikie, T.; Fang, Y.; Kadro, J. M.; Schreyer, M.; Wei, F.; Mhaisalkar, S. G.; Graetzel, M.; White, T. J. Synthesis and Crystal Chemistry of the Hybrid Perovskite $(CH_3NH_3)PbI_3$ for Solid-State Sensitised Solar Cell Applications. *J. Mater. Chem. A* **2013**, *1*, 5628.

(17) Protesescu, L.; Yakunin, S.; Bodnarchuk, M. I.; Krieg, F.; Caputo, R.; Hendon, C. H.; Yang, R. X.; Walsh, A.; Kovalenko, M. V. Nanocrystals of Cesium Lead Halide Perovskites ($CsPbX_3$, X = Cl, Br, and I): Novel Optoelectronic Materials Showing Bright Emission with Wide Color Gamut. *Nano Lett.* **2015**, *15*, 3692−3696.

(18) Stoumpos, C. C.; Malliakas, C. D.; Peters, J. a; Liu, Z.; Sebastian, M.; Im, J.; Chasapis, T. C.; Wibowo, A. C.; Chung, D. Y.; Freeman, A. J.; et al. Crystal Growth of the Perovskite Semiconductor $CsPbBr_3$: A New Material for High-Energy Radiation Detection. *Cryst. Growth Des.* **2013**, *13*, 2722−2727.

(19) Kondo, S.; Takahashi, K.; Nakanish, T.; Saito, T.; Asada, H.; Nakagawa, H. High Intensity Photoluminescence of Microcrystalline $CsPbBr_3$ Films: Evidence for Enhanced Stimulated Emission at Room Temperature. *Curr. Appl. Phys.* **2007**, *7*, 1−5.

(20) Song, J.; Li, J.; Li, X.; Xu, L.; Dong, Y.; Zeng, H. Quantum Dot Light-Emitting Diodes Based on Inorganic Perovskite Cesium Lead Halides ($CsPbX_3$). *Adv. Mater.* **2015**, n/a.

(21) Nitsch, K.; Hamplová, V.; Nikl, M.; Polák, K.; Rodová, M. Lead Bromide and Ternary Alkali Lead Bromide Single Crystals — Growth and Emission Properties. *Chem. Phys. Lett.* **1996**, *258*, 518−522.

(22) Nikl, M.; Nitsch, K.; Fabeni, P.; Pazzi, G. P.; Gurioli, M.; Santucci, S.; Phani, R.; Scacco, a; Somma, F. Luminescence of $CsPbBr_3$ -like Quantum Dots in CsBr Single Crystals. *Phys. E* **1999**, *4*, 323−331.

(23) de Quilettes, D. W.; Vorpahl, S. M.; Stranks, S. D.; Nagaoka, H.; Eperon, G. E.; Ziffer, M. E.; Snaith, H. J.; Ginger, D. S. Impact of Microstructure on Local Carrier Lifetime in Perovskite Solar Cells. *Science* **2015**, *348*, 683.

(24) Shi, H.; Du, M.-H. Shallow Halogen Vacancies in Halide Optoelectronic Materials. *Phys. Rev. B: Condens. Matter Mater. Phys.* **2014**, *90*, 1−6.

(25) Brine, H.; Sánchez-Royo, J. F.; Bolink, H. J. Ionic Liquid Modified Zinc Oxide Injection Layer for Inverted Organic Light-Emitting Diodes. *Org. Electron.* **2013**, *14*, 164−168.

(26) Yang, X.; Mutlugun, E.; Dang, C.; Dev, K.; Gao, Y.; Tan, S. T.; Sun, X. W.; Demir, H. V. Highly Flexible, Electrically Driven, Top-Emitting, Quantum Dot Light-Emitting Stickers. *ACS Nano* **2014**, *8*, 8224−8231.

(27) Galisteo-López, J. F.; Anaya, M.; Calvo, M. E.; Míguez, H. Environmental Effects on the Photophysics of Organic−Inorganic Halide Perovskites. *J. Phys. Chem. Lett.* **2015**, *6*, 2200−2205.

DOI: 10.1021/acs.jpclett.5b02011
J. Phys. Chem. Lett. 2015, 6, 4360−4364